

Electronic Supplemental Information

High-precision nanofabrication technology for metal nanoparticle ensembles using nanotemplate-guided thermal dewetting

Yusuke Niimura,^a Naoto Oonishi,^a Kyohei Okubo,^b Loan Le Thi Ngoc,^c and Edwin T. Carlen^{*ad}

* Corresponding author: Edwin T. Carlen, ecarlen@aichmis.com

^a University of Tsukuba, Graduate School of Pure and Applied Sciences, Tsukuba, Japan

^b Tokyo University of Science, Department of Materials Science and Technology, Tokyo, Japan.

^c Quy Nhon University, Physics Department, Quy Nhon City, Binh Dinh, Vietnam

^d Aichmis Technologies, Ann Arbor, Michigan, USA

S1. Nanofabrication

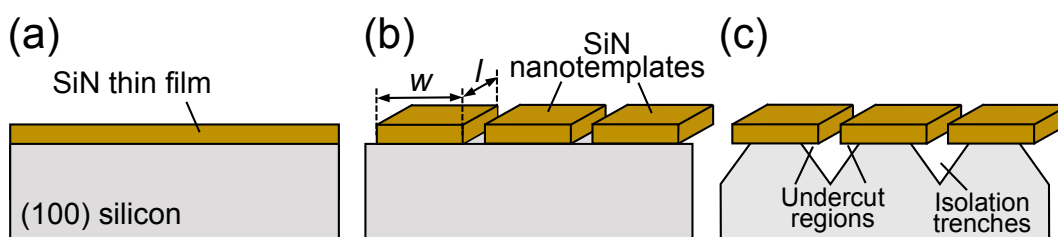


Figure S1 Fabrication process for silicon-nitride (SiN) nanotemplates. (a) Low-pressure chemical deposition of SiN thin film. (b) Nanopattern and etch SiN nanotemplates. (c) Anisotropic wet etch of silicon (Si) substrate.

Silicon wafers (100) were cleaned prior to deposition of a 40 nm-thick silicon-nitride (SiN) thin film with low-pressure chemical deposition (Fig. S1(a)). The SiN surface was then cleaned and activated with an oxygen plasma treatment (Pressure: 30 Pa, Power: 100 W, Time: 1 min). The nanotemplates were patterned using electron-beam lithography (ELS-750EX, Elionex) (Accel. voltage: 50 keV, Beam current: 10 pA, Field size: 600 μm^2 , Dose: 110 $\mu\text{C}/\text{cm}^2$) with ZEP520A resist (Zeon Corp.) (Diluted with ZEP-A at a weight ratio of 1:1.4) spin cast at 4000 rpm for 120 sec and soft baked at 180°C for 3 min. on a hotplate. The exposed resist was developed with ZED-N50 developer (Zeon Corp.). After development, an oxygen plasma step was used to descum the SiN surface (Pressure: 30 Pa, Power: 100 W, and Time: 10 sec). Reactive-ion etching (RIE-10NR, Samco) was used to selectively etch the exposed SiN in the nanogap regions (CHF_3 flow rate: 20 sccm, Pressure: 2 Pa, Power: 100 W, Time: 3 min) (Fig. S1(b)). Dilute aqueous potassium hydroxide (KOH) etchant was used to anisotropically etch the isolation trenches. Prior to KOH etching, the native silicon oxide was removed from the silicon surface using a 5-vol% hydrofluoric acid aqueous solution at room temperature for 1 min and immediately rinsed in deionized water at room temperature for 1 min. The samples were etched in a 0.5-wt% KOH aqueous solution heated at 40°C for 3 min, and subsequently rinsed in deionized water for 1 min and dried (Fig. S1(c)). A silicon-dioxide layer was grown on the exposed silicon surface following KOH etching and prior to gold deposition by heating the substrate at 1100°C for 30 min. The silicon-dioxide surface passivation prevents alloying of the silicon with the gold thin film (the silicon-gold eutectic temperature is 370°C). Polycrystalline gold thin films were deposited by sputtering (Pressure: 10^{-3} Pa and Rate: 0.06 nm/sec) or electron-beam evaporation (Pressure: 10^{-5} Pa and Rate: 0.1 nm/sec). The nanotemplate-guided thermal dewetting process was done in a muffle furnace (KDF S-70, Denken) using a three-step process: 1. Ramp-up: 30 min, 2. Dwell: 1100°C for 60-120 min, and 3. Ramp-down to room temperature. Following the thermal dewetting process, the surfaces were imaged using scanning electron microscopy.

S2. Imaging and data processing

The nanopatterned template surfaces and gold nanoparticle ensembles were imaged using a scanning electron microscope (SEM) (SU-8020 field emission electron microscope, Hitachi High-Tech. Corp.). The nanoparticle dimensions were estimated directly from the SEM images and corresponding scale bars.

S3. Nanoparticle diameter

The nanoparticle diameter can be controlled by adjusting the thickness of the polycrystalline gold thin film or by changing the areal dimensions of the nanotemplate. Using the former method, the mean nanoparticle diameter is estimated from empirical data, shown in Fig. S2, as $d_{NP} \approx 5.2 \times 10^{-5} V_{Au}$, where $V_{Au} = length \times width \times t_{Au}$ is the nominal volume of the sputter deposited polycrystalline gold island of thickness t_{Au} on a nanotemplate with in-plane dimensions $length$ and $width$. For example, a 100 nm-thick polycrystalline gold film on a $200 \times 200 \text{ nm}^2$ nanotemplate results in a mean nanoparticle diameter of approximately 200 nm, and 10 nm-thick gold film results in a mean nanoparticle diameter of approximately 20 nm.

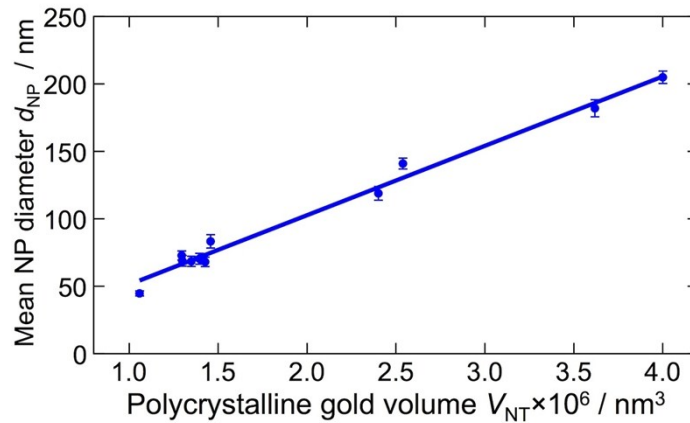


Figure S2 Measured mean nanoparticle (NP) diameter d_{NP} as a function of the volume of polycrystalline gold sputter deposited on the nanotemplate V_{NT} (Error bars: ± 1 SD, $n=50$).

S4. Residual gold in isolation trenches

Following sputtering of a polycrystalline gold thin film on the nanotemplate surfaces and subsequent annealing, we discovered that residual gold in the *v-shaped* isolation trenches *moves* to wider (and deeper) trench regions and eventually agglomerates into large nanoparticles. This phenomenon is caused by the *flow* of residual gold during the dewetting process, shown in SEM of Fig. S3(a). Figure S3(b, top) depicts the top-view of a nanotemplate array (dark gray rectangles), and Fig. S3(b, bottom) a side-view of the shallow and deep *v-shaped* isolation trenches. Figures S3(c) and S3(d) show SEM images of oligomer nanoparticle ensembles with large agglomerated nanoparticles in the deep trench regions following the thermal dewetting process.

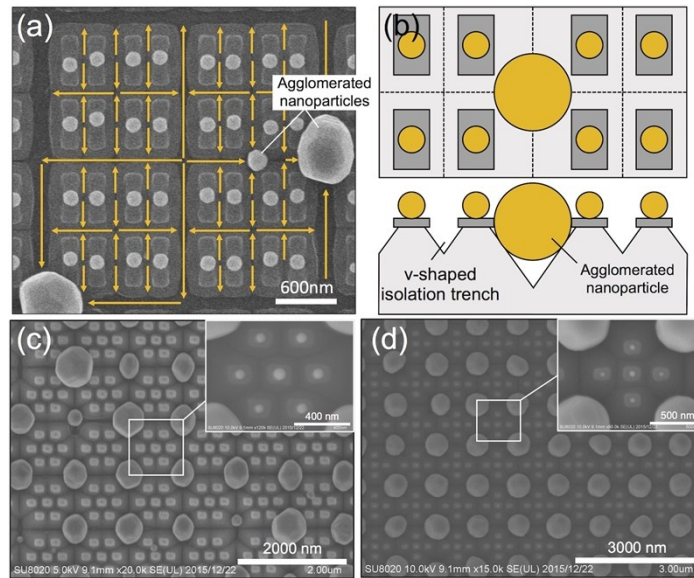


Figure S3 (a) Arrows indicate the flow of residual gold from shallow (narrow) trenches to deeper (wide) trenches and large agglomerated nanoparticles in the deeper (wide) trenches. (b) Top: top-view of nanotemplates, Bottom: side-view of nanotemplates showing shallow and deep v-shaped isolation trenches. (c) Agglomerated gold nanoparticles on the heptamer nanoparticle ensemble. (d) Agglomerated gold nanoparticles on the pentamer nanoparticle ensemble.

Based on this interesting phenomenon, we designed nanotemplate patterns that prevent the agglomeration of large nanoparticles near the nanotemplates by transporting (via flowing) the residual gold in the isolation trenches to the periphery of nanoparticle assembly during the dewetting the process. Figure S4(a) shows a SEM image of a nanotemplate array with deep reservoir structures located at the four corners of the patterned region. We expected that gold would flow and agglomerate in the reservoirs during the dewetting process. A 60 nm-thick polycrystalline gold thin film was sputtered on the nanotemplate surface and thermally annealed at 1100°C for 120 min. The SEM image in Fig. S4(b) shows that indeed most of the residual gold agglomerated into large nanoparticles in the corner reservoirs, however several agglomerated nanoparticles remain trapped on the array surface. The nanoparticles have a mean diameter of (119 ± 6) nm (± 1 SD, $n=50$) with corresponding coefficient of variation of $cv_d=5\%$, which was estimated from the histogram in Fig. S4(c). The spatial variation of the nanoparticle position is similar to data shown in Fig. 4 of the main article.

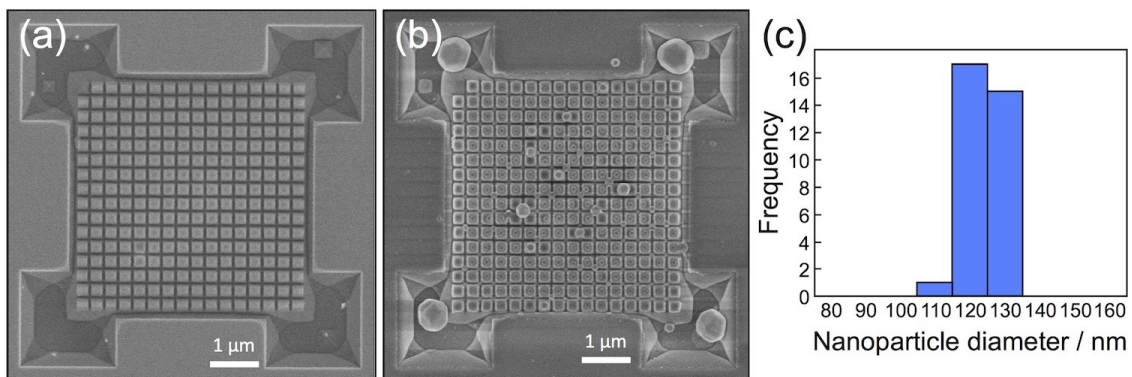


Figure S4 (a) SEM image of a 16×16 array of nanotemplates with large reservoirs at the four corners for collecting agglomerated nanoparticles. (b) SEM image of array following thermal dewetting of a 60 nm-thick polycrystalline gold thin film. (c) Histogram of the gold nanoparticle diameters ($n=50$).

S5. Glancing-angle deposition

Glancing-angle deposition in a high-vacuum evaporation deposition system can be used to prevent deposition of residual gold in the isolation trenches located between adjacent nanotemplates. Figure S5(a) schematically shows the deposition process. A 50 nm-thick gold thin film was deposited using electron-beam evaporation (Pressure: 10^{-5} Pa, Rate: 0.1 nm/sec) with an incidence angle of $\theta=70^\circ$ and array alignment angle $\alpha=45^\circ$ (see top right diagram in Fig. S5(a)). The corresponding SEM image is shown in Fig. S5(b, top). In this case, the variation of the gold nanoparticle position has increased with a mean offset of (47 ± 16) nm (± 1 SD, $n=50$), estimated from the histogram in Fig. S5(b, bottom left). In this case, we attribute the large offset distance to two factors. First, a glancing angle of 70° , with respect to normal incidence, and an array alignment angle of $\alpha=45^\circ$ (Fig. S5(a), upper right inset) results in non-uniform polycrystalline gold films on the nanotemplates that is thicker at the upper-left corner, thus introducing an offset bias to each nanotemplate. The second factor is the small nanoparticle diameter compared to the area of nanotemplate. We have investigated the relationship between the area of the nanotemplate and the nanoparticle diameter, and found that the mean offset distance increases substantially as the area of the nanotemplate is increased, with respect to the nanoparticle diameter. We find the optimal positioning precision is achieved with a square nanotemplate and a nanoparticle diameter $d_{NP}\approx s_{NT}$, where s_{NT} is the in-plane length of a side of a square nanotemplate.

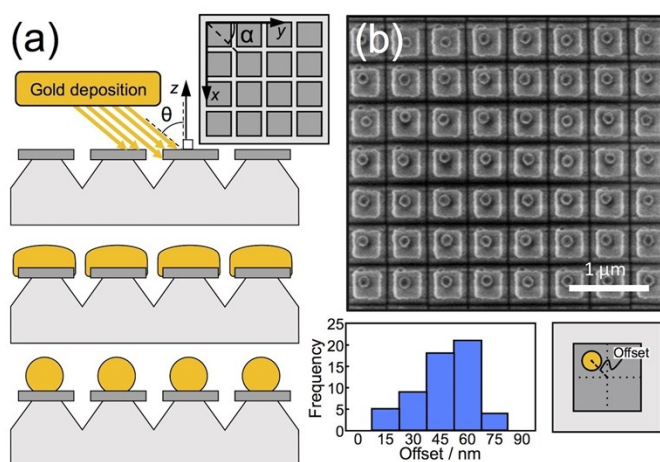


Figure S5 (a) Schematic diagram of glancing-angle deposition of gold to prevent residual gold in the trenches. Incidence angle $\theta=70^\circ$ and array alignment angle $\alpha=45^\circ$. (b) Top: SEM image of gold nanoparticle array following thermal annealing at 1100°C for 120 min. Bottom left: Histogram of offset distance from the center of the SiN template. ($n=50$) Bottom right: Dashed line represents the offset distance from the center of the SiN template to the center of the gold nanoparticle.

S6. Nanoparticle position

The precision of positioning a nanoparticle on the nanotemplate is dependent on the diameter of the nanoparticle with respect to the in-plane surface area of the nanotemplate. Figures S6(a) and S6(b) show an example of nanoparticle position on a square template of comparable dimensions. Figure S6(a) shows a SEM image of a periodic nanoparticle array with square nanotemplates of in-plane dimensions of $s_i \equiv \text{length} = \text{width} = 200$ nm and nanoparticles formed following thermal dewetting of a 100 nm-thick polycrystalline gold thin film. In this case, the mean diameter is (202 ± 6) nm (± 1 SD, $n=50$) with coefficient of variation of $cv_d=3\%$, and since the mean diameter is of similar dimension to the nanotemplate, i.e. $d_{NP}\approx s_i$, the mean offset (10 ± 6) nm (± 1 SD, $n=50$) is very small, estimated from the histogram in Fig. S6(b).

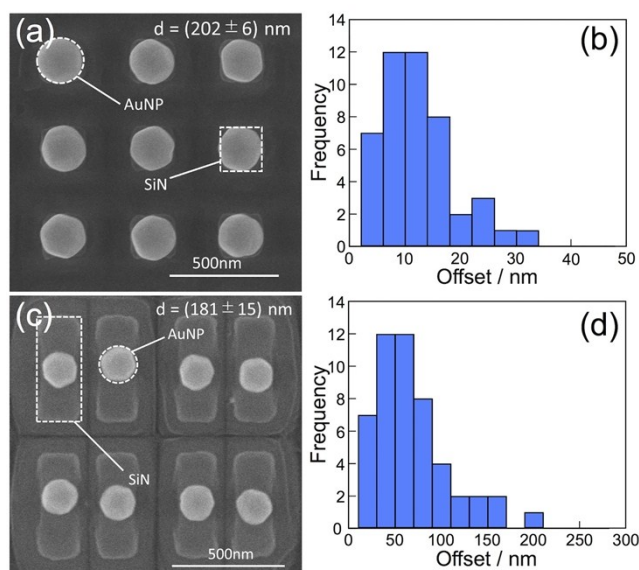


Figure S6 (a,b) Nanoparticle array with square nanotemplates ($length=width=200 \text{ nm}$) and 100 nm-thick polycrystalline gold thin film. (a) SEM image nanoparticle array. (b) Histogram of nanoparticle offset from template center ($n=50$). (c,d) Nanoparticle array with rectangular nanotemplates ($length=700 \text{ nm}$ and $width=170 \text{ nm}$) and 100 nm-thick polycrystalline gold thin film. (c) SEM image of a nanoparticle array. (d) Histogram of nanoparticle offset from template center ($n=50$).

Figures S6(c) and S6(d) show analysis results of nanoparticle position on a rectangular nanotemplate. Figure S6(c) shows a SEM image of a periodic nanoparticle array with in-plane rectangular nanotemplate dimensions $length=700 \text{ nm}$ and $width=170 \text{ nm}$ and nanoparticles formed following thermal dewetting of a 100 nm-thick polycrystalline gold thin film. The mean diameter is $(181 \pm 15) \text{ nm}$ ($\pm 1 \text{ SD}$, $n=50$) with coefficient of variation of $cv_d=8\%$. In this case, the $length$ of the nanotemplate is much larger than the nanoparticle diameter, which results in a significantly increased mean offset from the template center of $(59 \pm 39) \text{ nm}$ ($\pm 1 \text{ SD}$, $n=50$), estimated from the histogram in Fig. S6(d). Based on these preliminary results, we conclude that in order to achieve the highest precision nanoparticle position the nanotemplate dimensions should be of comparable size as the nanoparticle diameter, i.e. $d_{NP} \approx s_t$.

S7. Nanocavities

An important feature of a nanofabrication technology for nanoplasmonics applications, such as field-enhanced photochemistry and spectroscopy, is the ability to realize nanocavities with sub-20 nm nanogaps between adjacent nanoparticles. We have achieved nanogaps down to $g \approx 5 \text{ nm}$ using a dimer ensemble, shown in Fig. S7, which further supports the general suitability of this hybrid nanofabrication technology for nanoplasmonics applications.

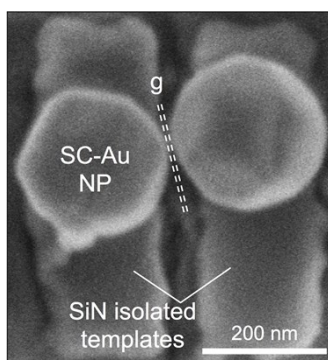


Figure S7 Example of nanoparticle dimer with a nanogap of $g \approx 5 \text{ nm}$.